Design of Chemoresponsive Liquid Crystals through Integration of Computational Chemistry and Experimental Studies

Tibor Szilvási[†], Luke T. Roling[†], Huaizhe Yu[†], Prabin Rai[‡], Sangwook Choi[†], Robert J. Twieg^{‡,*}, Manos Mavrikakis^{†,*}, Nicholas L. Abbott^{†,*}

ABSTRACT: We report the use of computational chemistry methods to design a chemically responsive liquid crystal. Specifically, we used electronic structure calculations to model the binding of nitrile-containing mesogens (4'-*n*-pentyl-4-biphenylcarbonitrile) to metal perchlorate salts (with explicit description of the perchlorate anion), which we call the Coordinately Saturated Anion Model (CSAM). The model results were validated against experimental data. We then used CSAM to predict that selective fluorination can reduce the strength of binding of nitrile-containing nematic LCs to metal salt-decorated surfaces and thus generate a faster reordering of LC in response to competitive binding of DMMP. We tested this prediction via synthesis of fluorinated compounds 3-fluoro-4'-pentyl[1,1'-biphenyl]-4-carbonitrile and 4-fluoro-4'-pentyl-1,1'-biphenyl, and subsequent experimental measurements of the orientational response of LCs containing these compounds to DMMP. These experimental measurements confirmed the theoretical predictions, thus providing the first demonstration of a chemoresponsive LC system designed from computational chemistry.

INTRODUCTION

Materials that can be programmed to respond to targeted chemical species, such as toxic industrial chemicals or chemical warfare agents, hold enormous potential in the context of designing new classes of actuators and sensors (e.g., wearable sensors). ¹⁻⁷ Liquid crystals (LCs) form the basis of one such promising approach, as they can be triggered to undergo ordering transitions in response to exposure to a range of targeted chemical species. ^{4,8-16} Specifically, by supporting micrometer-thick films of LCs on surfaces decorated with metal cations, ^{4,17} we and others have demonstrated that the competitive binding of the mesogens forming LCs and targeted chemical species with the cations can trigger LC ordering transitions. These LC ordering transitions are readily transduced by using optical and electrical methods. ¹⁸⁻²⁰

While experimental efforts over the past decade have realized chemoresponsive LCs that can report the presence of specific chemical targets, such as organophosphonates²¹⁻³³ or H₂S³⁴ introduced via partitioning from gas phases, one of the challenges underlying optimization of the design of chemoresponsive LC systems is exploration of the large number of experimental variables that define the LC materials and surface chemistries that lead to systems that respond sensitively and specifically to an analyte of interest. To address this challenge, as reported in this paper, we are exploring the integration of cycles of computational chemistry, organic synthesis, and physical property evaluation to efficiently design new chemoresponsive LCs.

Past experimental and computational studies have shown that the alignment of LCs supported on metal salt-decorated surfaces is dependent on coordination interactions between specific functional groups of the mesogens and the metal salts. ^{21,25,30} These studies revealed that both the identity and surface density of the metal cations (atoms per unit area or binding sites per unit area) are key design variables that influence the

responsiveness of the LCs. For example, Yang et al.²¹ found that nematic LC phases of 4'-n-pentyl-4-biphenylcarbonitrile (5CB) supported on perchlorate salts of metal cations with high electron affinities, such as Cu²⁺, Zn²⁺, Cd²⁺, Ni²⁺, Co²⁺, La³⁺, Al³⁺, Eu³⁺ or Fe³⁺, assume a homeotropic (perpendicular to the surface) orientation, whereas 5CB supported on salts of metal cations with low electron affinities, including Mn²⁺, Mg²⁺ and Na⁺, assume a planar or tilted orientation. The experimental studies also provided infrared spectroscopic evidence that competitive binding of organophosphonates (e.g., dimethylmethylphosphonate) to the metal cations could trigger surfacedriven ordering (anchoring) transitions in the LC films. More recently, these ideas were validated³⁵ by using electronic structure calculations to evaluate the thermochemical binding energies (BEs) of benzonitrile (PhCN, a surrogate molecule for 5CB) to metal cation centers. In addition, the magnitude of the difference in binding energies (ΔBE) of DMMP and PhCN to metal cations was shown to define a thermodynamic driving force for the experimentally observed anchoring transitions induced by DMMP: large magnitudes of ΔBE correlated with rapid anchoring transitions. More broadly, this past study validated the use of computational chemistry to describe existing chemoresponsive LCs and suggested that an opportunity exists to computationally-guide the design of new responsive material systems via (1) modification of the mesogen structure and (2) choice of surface metal cations. It is this opportunity that we address in the study reported in this paper.

The study reported in this paper leads to two important advances. First, the study further advances the computational description of chemoresponsive LCs by explicitly including the effects of metal salt anions in the calculations. This advance is motivated by past experimental observations that revealed that the choice of the salt anion (e.g., nitrate versus perchlorate) can influence the interaction of nitrile-containing mesogens with

[†] Department of Chemical and Biological Engineering, University of Wisconsin-Madison, 1415 Engineering Drive, Madison, Wisconsin 53706-1607, USA.

[‡] Department of Chemistry and Biochemistry, Kent State University, Kent, Ohio 44242, USA.

metal salt-decorated surfaces.³² We tested our new model, denoted here as the Coordinately Saturated Anion Model (CSAM), against experimental response times of nematic 5CB to DMMP using a range of different metal cations. We found that the CSAM more accurately describes the nature of the surface binding site, compared to the previously used models which did not explicitly include anions.³⁵

Second, we used the improved computational model to predict that the ortho-fluorine modification of 5CB (3-fluoro-4'pentyl[1,1'-biphenyl]-4-carbonitrile, FCB) should reduce the binding energy of the nitrile group to metal cations and thus (i) decrease the strength of the anchoring energy of the LC that causes the homeotropic orientation, and (ii) increase the thermodynamic driving force (ΔBE) for the displacement of the fluorinated mesogens by DMMP. The latter was predicted to lead to an increase in the rate of response of the LC to exposure to DMMP as compared to pure 5CB. We also used the model to predict that fluorophenyl compounds in which the nitrile group of 5CB was replaced by fluorine (e.g., 4-fluoro-4'-pentyl-1,1'biphenyl, F1), would not substantially bind to the metal cations, and thus should not influence the interfacial properties of the LC system (and thus responsiveness to DMMP). We tested these predictions by synthesizing the two fluorinated molecules FCB and F1, as shown in Figure 1. We characterized the orientations assumed by mixtures of F1 or FCB with 5CB on surfaces decorated with perchlorate salts of Fe3+, Al3+, Ga3+, La3+ and Zn²⁺, and quantified their response to DMMP. Importantly, the experimental observations were found to be in good agreement with the theoretical predictions, thus providing the first example of a chemoresponsive liquid crystal designed from computational chemistry.

NC
$$C_gH_{11}$$
 5CB

NC C_gH_{11} FCB

 C_gH_{11} FCB

Figure 1. Structures of 4'-*n*-pentyl-4-biphenylcarbonitrile (5CB), 3-fluoro-4'-pentyl[1,1'-biphenyl]-4-carbonitrile (FCB) and 4-fluoro-4'-pentyl-1,1'-biphenyl (F1) used in this study.

METHODS

Computational methods. Calculations using the CSAM were performed using the Gaussian 09 code. ³⁶ All geometry optimizations were performed at the PW91/def2-SVP level of theory, ^{37,38} and optimized geometries were confirmed with harmonic vibrational frequency calculations. From these optimized geometries, the M06-2X/def2-TZVP level of theory ³⁹ was used to perform more accurate single point calculations; these energies are reported in the main text. The choice of the method was determined by benchmark calculations using the highly accurate CBS-QB3 complete basis set method which we had used in previous models. ³⁵

The setup of CSAM structures was performed according to the following example: for Fe(ClO₄)₃ as the metal salt-decorated surface in the experimental system, one Fe³⁺ metal cation was used in the model. Fe³⁺ has six coordination sites³⁵ and each perchlorate anion can fill two coordination sites (see Figure 2a; left structure). Therefore, we used three perchlorates to fill all sites and thus form a Fe(ClO₄)₃ cluster. We confirmed computationally that adding a fourth perchlorate anion is energetically unfavorable. Zn²⁺, Al³⁺ and Ga³⁺ are also known to have six coordination sites, thus we used three perchlorate anions for each of these cations (the resulting clusters are structurally equivalent to the Fe(ClO₄)₃ cluster shown in Figure 2a). For La³⁺, because of the empty

d and f-orbitals, four perchlorate anions are needed to occupy all coordination sites (see Figure 2b; left structure), thus resulting in a negatively charged cluster [La(ClO₄)₄]¹. Formally, the additional fourth perchlorate used to achieve coordination saturation can be rationalized by sharing perchlorates between lanthanum ions, thus exploiting all 4 oxygens of a perchlorate ion.

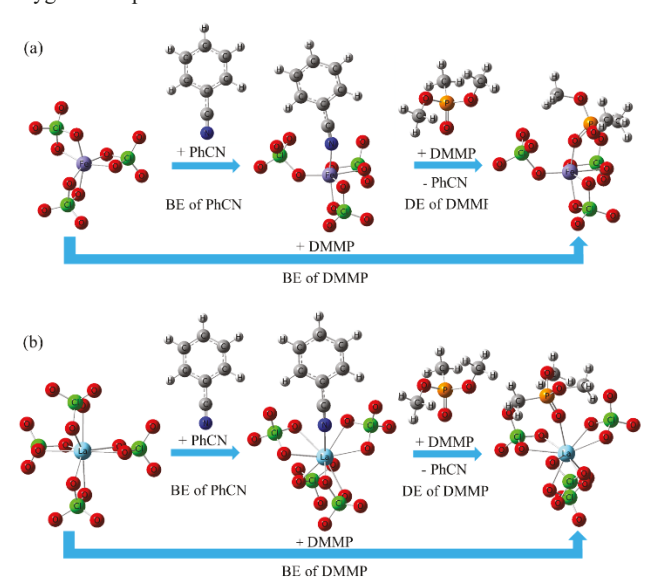


Figure 2. Representative structures from which binding energies (BE) and displacement energies (Δ BE) were calculated. (a) Coordinatively Saturated Anion Model (CSAM) structure for Fe(ClO₄)₃ (left structure) and Fe(ClO₄)₃ interacting with PhCN (middle structure) and DMMP (right structure). These structures were used to determine the BEs and Δ BE of PhCN and DMMP. (b) Coordinatively Saturated Anion Model (CSAM) structure of [La(ClO₄)₄] (left structure) and its interaction with PhCN (middle structure) and DMMP (right structure).

Binding energies (BEs) were calculated as the difference in total energy between the CSAM-mesogen complex ($E_{\rm CSAM-mesogen}$) and the isolated CSAM cluster ($E_{\rm CSAM}$) and the isolated mesogen ($E_{\rm mesogen}$), i.e., $BE_{\rm mesogen}=E_{\rm CSAM-mesogen}-E_{\rm CSAM}-E_{\rm mesogen}$. The binding of DMMP to the CSAM cluster was calculated in a similar manner. The minimum energy structures corresponding to the binding energy calculations for the Fe and La CSAM models are shown in Figure 2. By this convention, more negative BEs correspond to stronger interactions. As a result, when BE_{DMMP} is more negative than $BE_{mesogen}$, displacement of the mesogen from its bound state at the metal surface by DMMP should occur. This binding energy difference between mesogen and DMMP (Δ BE) can be compared with experimental response times as a shorter response time implies a larger thermodynamic driving force and thus larger binding energy difference. 35

Materials. The precursors, 4-bromo-2-fluorobenzonitrile and 4-npentylphenylboronic acid, were purchased from Combi-Blocks (San Diego, CA) and potassium carbonate, 1,4-dioxane, and polyethylene glycol (PEG 2000, molecular weight 2000 Da); were bought from Alfa Aesar (Ward Hill, MA). The 1-bromo-4-fluorobenzene, sodium carbonate, sym-dimethylethylene diamine, CuI, and diglyme were purchased from Acros. Pd(OAc)₂ and PdCl₂ for the synthesis of Pd(PPh₃)₄ were bought from Pressure Chemical (Pittsburgh, PA). 5CB was purchased from EMD Chemicals (Hawthorne, NY). SU-8 2050 and SU-8 developer were purchased from MicroChem (Westborough, MA). Cylopentanone was purchased from Sigma Aldrich (Milwaukee, WI). Perchlorate salts of metal ions (Zn, La, Al, Fe, Ga) in their highest purity form were purchased from either Sigma Aldrich or Alfa Aesar. The tridecafluoro-1,1,2,2-tetrahydrooctyl)-trichlorosilane was purchased from Gelest (Morrisville, PA). DMMP in nitrogen at a concentration of 10 ppmv was obtained from Airgas (Radnor, PA) and used as received.

Synthesis of 3-fluoro-4'-pentyl[1,1'-biphenyl]-4-carbonitrile (FCB).⁴¹ Potassium carbonate (4.78 g, 34.57 mmol) was placed in a two-neck flask and 10 mL water was added and stirred until a clear solution was obtained. Next, 1,4-dioxane (90 mL) was added to this solution, which was degassed by bubbling with nitrogen for 15 minutes. To this degassed solution were added 4-bromo-2-fluorobenzonitrile (3.46 g, 17.28 mmol) and 4-pentylphenylboric acid (4.32 g, 22.47 mmol, 1.3 equiv) followed by palladium tetrakistriphenylphosphine (0.6 g, 0.52 mmol). The solution was stirred overnight at 90°C. The reaction was monitored by TLC, which indicated the complete consumption of the starting materials. The reaction mixture was poured into ice water (200 mL) and stirred. The organic compound was extracted with ethyl acetate which was washed with water, brine and dried over MgSO₄. The excess solvent was removed under reduced pressure. The crude product was further purified by column chromatography using hexane-ethyl acetate solution (9:1) to afford a yellow liquid. The yellow color of the product was removed by treating with activated charcoal, filtering through a pad of silica gel and washing with DCM. The solvent was removed under reduced pressure to afford a faint vellow liquid (4.00 g, 86%); ¹H NMR (CDCl₃, 400 MHz) δ 7.49 (dd, J =8.0 Hz, 6.4 Hz, 1H), 7.46 (d, J = 10.4 Hz, 2H), 7.44 (dd, J = 8 Hz, 1.6 HzHz, 1H), 7.36 (dd, J = 10.4 Hz, 1.6 Hz, 1H), 7.27 (d, J = 8.4 Hz, 2H), 2.66 (t, J = 4.6 Hz, 2H), 1.65 (quint, J = 6.0 Hz, 2H), 1.36-1.35 (m, 4H), 0.90 (t, J = 6.8 Hz, 3H); ¹²C NMR (CDCl₃, 100 MHz) δ 163.4 (d, J = 258.3 Hz), 148.5 (d, J = 8.15 Hz), 144.6, 135.3, 133.6, 129.3, 127.0, 123.1 (d, J = 3.0 Hz), 114.5, 114.3 (d, J = 2.9 Hz), 99.3(d, J = 15.6 Hz), 35.62, 31.48, 31.03, 22.53, 14.02; ¹⁹F NMR (CDCl₃, 75 MHz) δ 106.37 (dd, J = 10.37 Hz, 6.68 Hz, 1F).

Synthesis of 4-fluoro-4'-pentyl-1,1'-biphenyl (F1).42 A stirred mixture of sodium carbonate (1.46 g, 13.75 mmol), Pd(OAc)₂ (13.9 mg, 1 mol%), PEG 2000 (25 g) and water (20 mL) was heated to 50°C. Next, 1-bromo-4-fluorobenzene (1.23 g, 7.0 mmol) and 4-pentylphenylboronic acid (2.0 g, 10.41 mmol) were added to the reaction mixture which was heated and stirred for 2 hours. The reaction mixture was cooled to room temperature and the resulting suspension was extracted with diethyl ether. The organic layer was filtered through a thin silica pad and the excess solvent was removed under reduced pressure to afford the desired product (quantitative). The slight yellowish color was then removed by column chromatography using hexane as eluent (yield 1.67 g, 98%); m.p. 40.6°C; ¹H NMR (400 MHz, CDCl₃) δ 7.51-7.49 (m, 2H), 7.44 (dd, J = 8.0 Hz, 1.6 Hz, 2H), 7.24 (d, J = 4.4 Hz, 2H), 7.11-7.01 (m, 2H), 2.63 (t, J = 7.6 Hz, 2H), 1.66 (quint, J = 7.6Hz, 2H), 1.36-1.33 (m, 4H), 0.90 (t, J = 6.8 Hz, 3H); ¹³C NMR (100 MHz, CDCl₃) δ 162.3 (d, J = 244.4 Hz), 142.1, 137.6, 137.3, 128,9, 128.5, 126.8, 115.5 (d, J = 21.22 Hz), 35.5, 31.5, 31.2, 22.6, 14. 0; ¹⁹F NMR (75 MHz, CDCl₃), -114.31 to -114.38 (m, 1F).

Formation of thin films of LC supported on metal salt-decorated surfaces. The films of LC were formed within polymeric microwells. The fabrication of the microwells has been described previously. 43 Additional details are provided in the Supporting Information. Metal perchlorate salts were dissolved into dry ethanol at the desired concentration, and then 50 μ L of the solution was deposited by spin-coating (3000 rpm for 30s) onto the glass surfaces at the bottom of the polymeric microwells. Next, the microwells were filled with LC by depositing 2 μ L of LC onto each array of microwells using a micropipette. The excess LC was removed from the array by wicking into a microcapillary.

Formation of LC optical cells from glass substrates. Metal salts were deposited onto glass substrates by spin coating ethanolic solutions (100 $\mu L)$ of metal perchlorates (0.1-0.5 mM). Two metal salt-coated substrates were aligned facing each other, spaced apart using a film of Mylar with a thickness of 12.5 μm , and then held together using binder clips. Next, 2 μl of 5CB was drawn by capillarity into the cavity between the two surfaces of the optical cell.

Optical characterization of LC films. The optical appearance of the LC was characterized by using an Olympus BX-60 polarizing light microscope in transmission mode (Olympus, Japan). Conoscopic imaging of the LC films was performed by inserting a Bertran lens into

the optical path of a polarized-light microscope to distinguish between homeotropic and isotropic films.⁴⁴

Ordering transition induced by DMMP. The LC-filled microwells were exposed to a stream of dry N_2 containing DMMP (10 ppm) within a flow cell with glass windows that permitted characterization of the optical appearance of the LC using a polarized optical microscope. A detailed description of the flow cell can be found in earlier publications. The gas containing DMMP was delivered to the flow cell at 300 ml/min by using a rotameter (Aalborg Instruments and Control, Orangeburg, NY). The optical appearance of the LC film was recorded using an Olympus camera (Olympus C2040Zoom, Melville, NY) and WinTV software (Hauppauge, NY). The optical response of each LC film to DMMP was normalized by the maximum response (maximum intensity of transmitted light). The onset of exposure of the LC film to DMMP is denoted as t=0 s in the plots reported in this paper. Error bars (standard deviations) are calculated from 5 repeat experiments unless stated otherwise.

RESULTS AND DISCUSSION

One important conclusion of our prior computational work³⁵ was that charge transfer between the metal cations and their immediate environment (e.g., the counter ion and/or residual solvent such as ethanol) modulates the strength of binding of 5CB to the metal cations. This conclusion was supported by experimental studies in which the orientations of nematic films of 5CB were studied on metal salt surfaces with different anions.³² Whereas our previous computation model did not explicitly include the anions (the charge of the cation was lowered to account for charge transfer from the anion; referred to below as the Reduced Charge Model), in our new model (the CSAM), we explicitly add counter ions to saturate the coordination shell of the metal cation (Figure 2). Explicit inclusion of the anion was performed to provide a more detailed representation of the environment around the metal cation and thus a more accurate calculation of binding energies (see details in the Methods section). As previous experimental studies demonstrated that surfaces decorated with perchlorate salts of metal cations with high electron affinities, such as Zn²⁺, La³⁺, Al³⁺, and Fe³⁺, induce a homeotropic orientation of nematic 5CB,21 as shown in Table 1, we selected metal cations with high electron affinities to validate our new computational model.

Table 1. Binding energies of nitrile and fluorine-substituted mesogens to metal cations, evaluated using the Coordinately Saturated Anion Model on surrogate molecules. Anions are perchlorates. Displacement energies (in parenthesis) are calculated as the difference between DMMP and mesogen binding energies. All energy values are in eV.

Experi- mental molecule	Theoreti- cal model structure	A1 ³⁺	Fe ³⁺	Ga ³⁺	La ³⁺	Zn ²⁺
5CB		-0.95 (-0.81)	-0.93 (-0.72)	-1.06 (-0.72)	-0.71 (-0.54)	-0.53 (-0.40)
FCB	N N	-0.91 (-0.84)	-0.89 (-0.76)	-1.01 (-0.76)	-0.66 (-0.59)	-0.48 (-0.45)
F1	○ F	-0.03 (-1.73)	-0.03 (-1.62)	-0.06 (-1.72)	-0.04 (-1.21)	-0.05 (-0.88)
DMMP	0 0 0 0	-1.76	-1.65	-1.78	-1.25	-0.93

The molecular models used in our calculations include only the terminal aromatic ring of the mesogen, and thus PhCN serves as a surrogate for 5CB (Table 1, Figure 2). This simplification was implemented to minimize computational cost. To evaluate the appropriateness of this simplification, we show a charge density difference plot for PhCN bound to Fe³⁺ in Figure 3 (left). The plot shows regions where charge density increased or decreased relative to the free PhCN and Fe(ClO₄)₃ species as a result of the binding event. Figure 3 clearly shows that the charge density change is largely located on the iron and the nitrile group, and not the aromatic ring. It is reasonable to assume, therefore, that the second aromatic ring in 5CB plays an even smaller electronic role in the binding and that it can be neglected to a first approximation.

We calculated the binding energies of either PhCN or DMMP to metal cation clusters. All calculated binding energies are provided in Table 1. Inspection of Table 1 reveals that the calculated binding energies (BEs) are in the range of typical chemical interactions (order of 1.0 eV), which is an improvement relative to our previous Reduced Charge Model, 35 for which the BEs were calculated to be as high as $\sim\!\!8$ eV. Table 1 also shows the binding energy difference between PhCN and DMMP, which as noted above provides a thermodynamic driving force for the displacement of PhCN (and 5CB) by DMMP. The CSAM predicts that DMMP binds more strongly than 5CB to all metal cations, and that the thermodynamic driving force for displacement of 5CB by DMMP is ranked Al $^{3+}$ > Fe $^{3+}$ = Ga $^{3+}$ >La $^{3+}$ > Zn $^{2+}$.

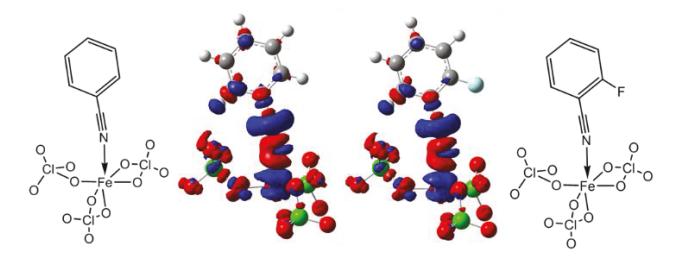


Figure 3. Charge density difference plots showing charge transfer that results from binding of PhCN, surrogate for 5CB (left, schematic representation is on the far left) and ortho-substituted PhCN, surrogate for FCB (right, schematic representation is on the far right) to an Fe(ClO₄)₃ model system. 5CB and FCB show almost identical charge density difference plots indicating very similar binding. Charge depletion is shown by blue regions, and charge accumulation by red. An isosurface of 0.0015 e/Å³ was used to construct the charge density difference plot.

To test the above-described theoretical predictions for binding and displacement energies (Table 1), we performed LC microwell experiments using each of the metal perchlorate salts (details are described in the Methods section). Similar to past experimental results, we measured nematic 5CB on the metal salt-coated surfaces to adopt a homeotropic orientation (left side of Figure 4a). This result is consistent with calculated binding energies of -0.55 to -1.06 eV for 5CB in Table 1. In addition, we exposed the oriented nematic films of 5CB to gas streams containing 10 ppm of DMMP (details can be found in the Methods section), and quantified the dynamic response of the LC films to the DMMP by using polarized optical microscopy (right side of Figure 4a). Inspection of Figure 4b reveals that the response times of the 5CB ranked $Fe^{3+} < Al^{3+} \sim Ga^{3+} < La^{3+} <$ Zn²⁺. Figure 4c compares the time taken for each LC film to reach 80% of its full response to DMMP. A two-sided Student's t-test with a 95 % confidence interval confirmed the statistically significant difference between the responses of Zn²⁺ and La³⁺

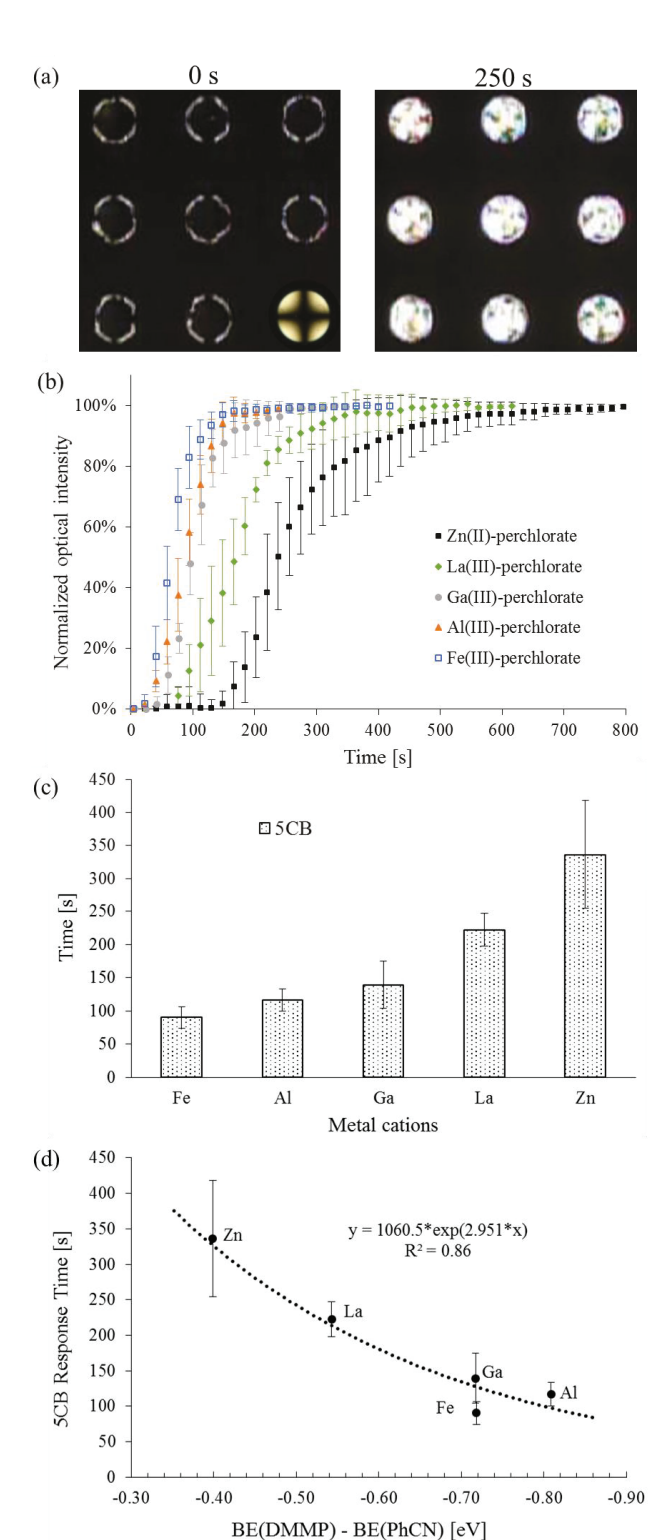


Figure 4. (a) Polarized micrographs of representative microwells prepared using nematic 5CB and La³⁺, recorded at the start of the experiment (time = 0 s) and at the end of the of the experiment (time = 250 s). (b) Average normalized intensity of polarized light transmitted through 5CB supported on 10 mM metal salt films and then exposed to a vapor of 10 ppm DMMP at 0 s. (c) Response times of pure 5CB to DMMP. The response time is defined as the time required to reach 80% normalized light intensity. (d) Response time of 5CB to DMMP as a function of the calculated difference in binding energies (BE) of DMMP and 5CB to the respective metal salts.

(t-value = 0.001) and La³⁺ and Ga³⁺ (t-value = 0.004). However, there is no statistical difference between Al3+ and Ga3+ (t-value = 0.16) or Fe³⁺ and Al³⁺ (t-value = 0.054). Previously, we presented a simple model that predicts response times and binding energy differences to follow an exponential relationship. 35 Consistent with this prediction, Figure 4d shows that experimental measurements of the response times do follow an exponential change with the binding energy difference, with the apparent exception of Fe³⁺. We note, however, that the above reported statistical analysis indicated that there was no significant difference between the response times of Al³⁺ and Ga³⁺, as reflected in the error bars of the data shown in Figure 4d. In addition, we note that the uncertainty in the calculated binding energies involving the Fe³⁺ cluster is likely to be larger than the other metal cations due to the open d-shell of Fe³⁺ (which is known to be more difficult to model in comparison with closed shell species).46

Overall, we interpret the results above to indicate that the CSAM provides a good description of the experimental response of 5CB (supported on metal cations) to DMMP. Next, we used the model to guide evaluation of modifications to the molecular structure of 5CB that would potentially lead to an increase in the responsiveness of the nematic LC to DMMP. Specifically, motivated by chemical intuition that the electronegative fluorine should withdraw electron density from the phenyl ring and its nitrile group, thereby weakening the binding of the molecule to the metal cation, we evaluated computationally the binding of an ortho-fluorine modification of PhCN (F-PhCN, which is the surrogate to FCB, see Fig. 1) to metal cation clusters. Table 1 shows that the CSAM predicts that fluorination decreases the binding energy of the nitrile group to all metal cations by 0.03-0.05 eV. Charge density difference plot analysis of F-PhCN (Figure 3) revealed that the regions of charge depletion and accumulation are generally similar for PhCN and ofluorine-PhCN, which is consistent with the modest change in binding energies caused by fluorine substitution. Close inspection of Figure 3, however, reveals that the region of charge accumulation is somewhat smaller for the F-PhCN. Finally, we comment that a change in binding energy of 0.06 eV corresponds (at room temperature) to an order of magnitude change in the binding equilibrium constant, and thus we would predict a change in binding energy of 0.03-0.05 eV to lead to a measurable effect.

For comparison, we also evaluated the binding of fluorobenzene (FB, which is the surrogate of F1, see Fig. 1) in which the nitrile group of PhCN is replaced with a fluorine atom. Table 1 shows that the binding energy of FB is approximately ~ 0.5 -1.0 eV weaker than PhCN, translating into a >8 order of magnitude difference in adsorption equilibrium constant. Based on this prediction, F1 would not be expected to be able to compete with 5CB for metal cation binding sites (in experiments performed with mixtures of F1+5CB, as described below).

Motivated by these computational predictions, two fluorinated molecules, FCB and F1, were synthesized using the procedures described in Scheme 1. Their identities were confirmed using ¹H, ¹³C, and ¹⁹F NMR (see Methods). Their phase transitions were observed using differential scanning calorimetry (DSC, Figure S2) and polarized optical microscopy (POM). While 5CB undergoes a phase transition from a nematic to an isotropic phase at 35.5 °C, we found that neither F1 nor FCB exhibited a nematic phase in pure form at ambient temperature. Because F1 and FCB are themselves not mesogenic, we added them to 5CB

to create nematic mixtures. DSC analysis confirmed that both F1 and FCB form homogeneous mixtures with 5CB (Figure 5; 95% wt/wt% 5CB and 5% wt/wt% F1 or FCB). Inspection of optical images of the mixtures using POM confirmed that the temperature of the transition from the nematic to isotropic phase ($T_{\rm NI}$) decreased linearly with increase in the wt% of F1 or FCB in the mixture (Figure S3). Mixtures that exhibited room temperature nematic phases contained less than 15 wt% F1 or 20 wt% FCB in 5CB, respectively. Accordingly, in the experiments reported below, we used LC mixtures containing 5 wt% of F1 or FCB in 5CB.

Scheme 1. Synthesis of 3-fluoro-4'-pentyl[1,1'-biphenyl]-4-carbonitrile (FCB) and 4-fluoro-4'-pentyl-1,1'-biphenyl (F1).

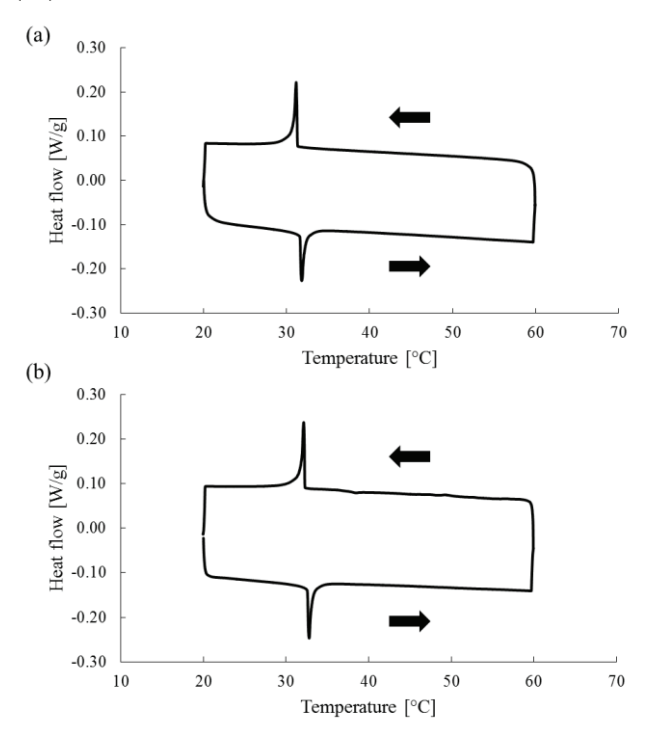


Figure 5. Differential scanning calorimetry (DSC) plots of (a) F1 mixture (95 wt% 5CB + 5 wt% F1) and (b) FCB mixture (95 wt% 5CB + 5 wt% FCB). Plots show only the nematic/isotropic transitions. The bottom line corresponds to heating and the upper line to cooling, as indicated by the arrows. DSC scan rate 2 °C/min.

First, we investigated the orientations assumed by mixtures containing 5 wt% of F1 or FCB in 5CB on Fe³⁺-decorated surfaces, as a function of the surface density of Fe³⁺ metal cation binding sites. We performed these experiments by depositing Fe³⁺ salts onto glass surfaces by spin-coating from ethanolic solutions containing 0.1 mM, 0.2 mM or 0.5 mM perchlorate salt. To assess the potentially complicating influence of the LC-air interface on the orientation assumed by the LC at the metal salt-coated surface, we performed these experiments using both microwells (Figure S7) and LC cells composed of two identically prepared surfaces (Figures S4-S6). Both experimental designs led to the same conclusions. As shown in Figure 6, when the surfaces were prepared with high surface densities of Fe³⁺ bind-

ing sites (0.5 mM Fe(ClO₄)₃), 5CB as well as the mixtures containing FCB and F1 adopted homeotropic orientations (0% intensity of transmitted light in Figure 6). Alternatively when the surfaces presented the lowest density of Fe³⁺ binding sites (0.1 mM Fe(ClO₄)₃), all LCs assumed orientations that were parallel to the surfaces (planar anchoring, indicated by high intensity of transmitted light). At intermediate densities of Fe³⁺ binding sites, however, we observed the mixture containing FCB and 5CB to adopt a planar orientation, whereas pure 5CB and the mixture of 5CB and F1 both adopted tilted orientations. We performed repeat experiments and statistical analyses to confirm the above conclusions (FCB+5CB versus F1+5CB were found to be statistically different using a t-test (t-value < 0.01). In contrast, there was no statistical difference between results obtained with 5CB+F1 and 5CB (t-value = 0.21). Importantly, also, the measured influence of FCB and F1 on the orientation of the LC mixtures is consistent with our computational predictions. Specifically, the planar orientation of the 5CB+FCB mixture (0.2mM) is consistent with the lower binding energy predicted for FCB as compared to 5CB. In addition, the absence of any measurable effect of F1 on the behavior of the mixture of F1+5CB (relative to 5CB) is consistent with the predicted absence of a significant binding energy for F1 to the metal cation.

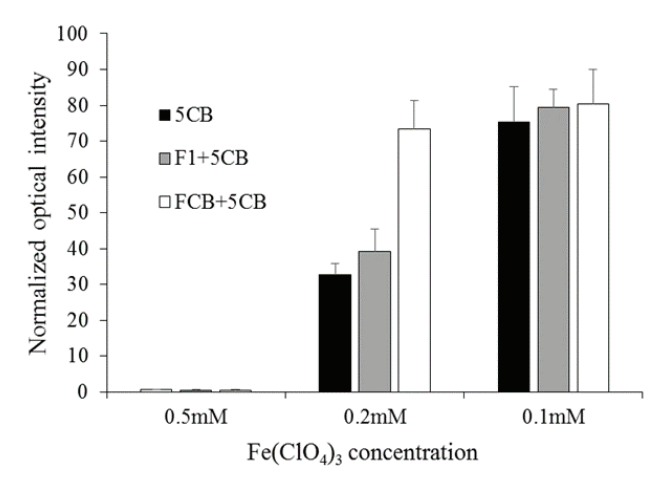


Figure 6. Normalized intensity of polarized light transmitted through pure 5CB, F1 mixture (95 wt% 5CB + 5 wt% F1), or FCB mixture (95 wt% 5CB + 5 wt% FCB), each held between two iron salt covered substrates prepared using 0.5 mM, 0.2 mM or 0.1 mM Fe(ClO₄)₃.

Next, we measured the response of the LC mixtures supported on Fe³⁺-decorated surfaces (prepared using 20 mM Fe(ClO₄)₃) to DMMP (10 ppm) to determine if the predicted influence of F1 and FCB on the LC binding energies was also evident in the response to DMMP. In these studies, we used surfaces presenting a density of metal cations that was well above that used in Figure 6 in order to obtain reproducible and uniform homeotropic alignment of the LCs. The time-dependent responses of pure 5CB, the F1+5CB mixture, and the FCB+5CB mixture to DMMP are shown in Figure 7a. Importantly, and consistent with our computational predictions, we measured the LC containing FCB to respond more quickly than pure 5CB. Furthermore, there was no substantial influence of F1, consistent with the predicted, very weak binding of F1 relative to 5CB to the metal salt-decorated surface.

Additionally, we performed a series of experiments in which we compared the DMMP-triggered responses of 5CB and mixtures of FCB+5CB, when the LCs were supported on surfaces decorated with 5 different metal perchlorate salts (Figure 7b). Aided by statistical analyses, we found the presence of FCB to have a significant effect on the response of the LC to DMMP for Fe³+ (t-value = 0.021), Ga³+ (t-value = 0.029) and La³+ (t-value = 0.041). However, the uncertainty in our experimental data led us to conclude that there is no statistically significant differences for Zn²+ (t-value = 0.11) or Al³+ (t-value = 0.24). We then performed an overall analysis using all metal cations. This analysis showed a robust difference between FCB and 5CB results (t-value = 0.01), consistent with our theoretical predictions.

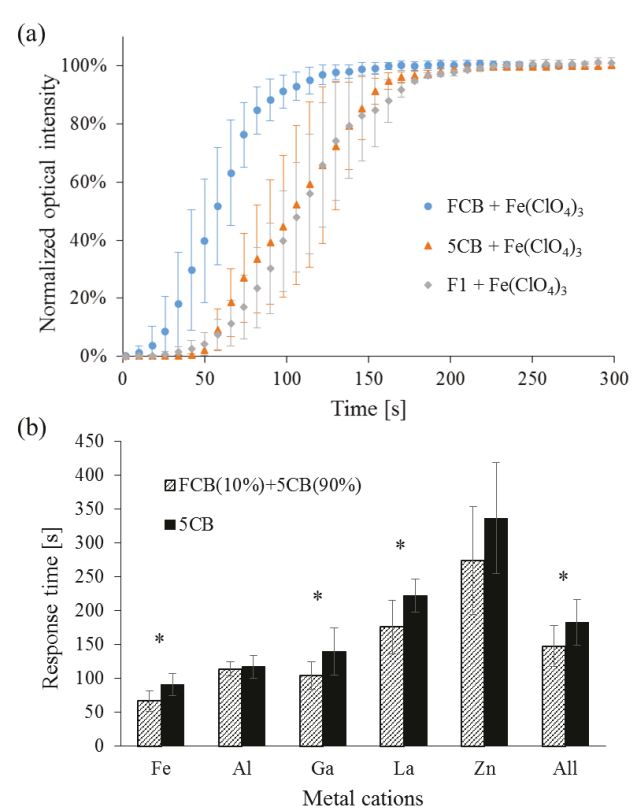


Figure 7. (a) Average normalized intensity of polarized light (crossed polars) transmitted through LC films (pure 5CB, F1 mixture (95 wt% 5CB + 5 wt% F1), and FCB mixture (95 wt% 5CB + 5 wt% FCB)) supported on surfaces coated with 20 mM Fe(ClO4)3 and then exposed to a vapor of 10 ppm DMMP at 0 s. (b) Response times of pure 5CB and FCB mixture (90 wt% 5CB + 10 wt% FCB) supported on surfaces coated with 10mM metal salts, following exposure to DMMP. The last column is an average over all metal cations. Asterisks indicate a statistically significant difference between 5CB and FCB+5CB results.

The results described above demonstrate that modula-tion of the binding interactions of LCs at surfaces via the use of fluorination offers a strategy for increasing the responsiveness of chemosensitive LCs. Although the magnitude of the change in the response time reported in this paper is modest, the result is significant in that it demonstrates that it is possible to guide the design of the improved chemoresponsive LCs via computational chemistry. Indeed, the computational model reported in this study predicted that the effect of fluorination on binding energy (FCB vs 5CB) to be \sim 0.05 eV, and the 10-20% decrease

in response time seen in Figure 7b is consistent with this computational prediction (see Figure 4d). We attribute the faster response observed in the experiments with the FCB+5CB mixture to the weaker binding of FCB molecules to the metal salt surface, and the preferential displacement of the bound FCB molecules by DMMP. We suggest that displacement of bound FCB triggers the optical transition observed in the experiments. Future studies will build from this successful demonstration of design methodology to identify additional modifications of 5CB that will modulate further the binding strength of the nitrile group to metal cations. More broadly, the application of theoretical models such as CSAM has the potential to lead to facile methods to design chemoresponsive LC materials because they minimize the need for slow and laborious experiments while also providing fundamental insights into the chemical interactions underlying functional properties.

CONCLUSIONS

This study describes the development of a methodology that permits the design of new chemoresponsive LC systems based on the integration of computational chemistry, organic synthesis, and physical characterization. By using a new model for metal cation binding sites that incorporates the presence of the perchlorate anions, we found that a thermodynamic driving force calculated as the difference in binding energies between an analyte (DMMP) and a mesogen (5CB) to metal cations correlated with the experimentally measured analyte-induced LC response dynamics. By using the validated model, we identified new fluorinated molecules that were predicted to have promise as chemoresponsive LC materials. We synthesized the molecules, and then verified by experiments that *ortho*-fluorine modification of 5CB increases the rate of response of a mixture of FCB and 5CB to DMMP. In contrast, a control compound called F1 was predicted by computations and verified experimentally to have no effect on the response time of LCs containing mixtures of F1 and 5CB. Overall, our approach demonstrates how computational chemistry can lead to the development of improved chemoresponsive systems based on LCs, including by providing guidance regarding the selection of metal salts and molecular structures of mesogens.

ASSOCIATED CONTENT

Fabrication of polymeric microwells, DSC results for 5CB, F1, and FCB, Phase transition temperature measurements of F1+5CB and FCB+5CB mixtures, Measurements of homeotropic ordering of 5CB, F1+5CB mixtures, and FCB+5CB mixtures, ¹H, ¹³C, and ¹⁹F NMR spectra of FCB and F1. This material is available free of charge via the Internet at http://pubs.acs.org.

AUTHOR INFORMATION

Corresponding Authors

* Email: rtwieg@kent.edu * Email: emavrikakis@wisc.edu * Email: nlabbott@wisc.edu

Notes

NLA declares a financial interest in Platypus Technologies LLC, a for-profit company that has developed LC-based analytic technologies. The other authors declare no competing financial interests.

ACKNOWLEDGMENT

This work was supported by the National Science Foundation (DMREF grant DMR-1435195) and the Army Research Office

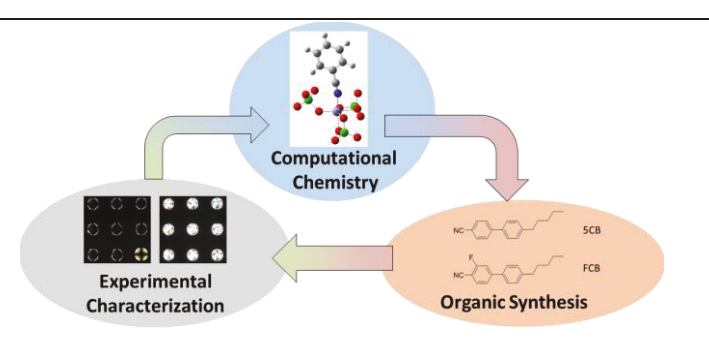
(W911NF-14-1-0140). Calculations were performed at supercomputing centers located at the Environmental Molecular Sciences Laboratory (EMSL), which is sponsored by the Department of Energy (DOE) Office of Biological and Environmental Research at Pacific Northwest National Laboratory (PNNL); the Center for Nanoscale Materials (CNM) at Argonne National Laboratory (ANL), supported by DOE Contract DE-AC02-06CH11357; and the National Energy Research Scientific Computing Center (NERSC), supported by DOE Contract DE-AC02-05CH11231. Facilities of the Wisconsin MRSEC were used in this work (DMR-1121288).

REFERENCES

- (1) Lashof, D. A.; Ahuja, D. R. Relative Contributions of Greenhouse Gas Emissions to Global Warming. *Nature* **1990**, *344*, 529-531.
- (2) Ashley, K. Developments in Electrochemical Sensors for Occupational and Environmental Health Applications. *J. Hazard. Mater.* **2003**, *102*, 1-12.
- (3) Hanrahan, G.; Patil, D. G.; Wang, J. Electrochemical Sensors for Environmental Monitoring: Design, Development and Applications. *J. Environ. Monit.* **2004**, *6*, 657-664.
- (4) Shah, R. R.; Abbott, N. L Principles for Measurement of Chemical Exposure Based on Recognition-driven Anchoring Transitions in Liquid Crystals. *Science* **2001**, *293*, 1296-1299.
- (5) Knapton, D.; Burnworth, M.; Rowan, S. J.; Weder, Fluorescent Organometallic Sensors for the Detection of Chemical-Warfare-Agent Mimics. *Angew. Chem. Int. Ed.* **2006**, *45*, 5825-5829.
- (6) Hu, X.-X.; Su, Y.-T.; Ma, Y.-W.; Zhan, X.-Q.; Zheng, H.; Jiang, Y.-B. A Near Infrared Colorimetric and Fluorometric Probe for Organophosphorus Nerve Agent Mimics by Intramolecular Amidation. *Chem. Commun.* **2015**, *51*, 15118-15121.
- (7) Ashley, J. A.; Lin, C.-H.; Wirsching, P.; Janda K. D. Monitoring Chemical Warfare Agents: A New Method for the Detection of Methylphosphonic Acid. *Angew. Chem. Int. Ed.* **1999**, *38*, 1793-1795.
- (8) Cachelin P.; Green, J. P.; Peijs, T.; Heeney, M.; Bastiaansen, C. W. M. Optical Acetone Vapor Sensors Based on Chiral Nematic Liquid Crystals and Reactive Chiral Dopants. *Adv. Optical Mater.* **2016**, *4*, 592–596.
- (9) Brake, J. M.; Daschner, M. K.; Luk, Y.-Y.; Abbott, N. L. Biomolecular Interactions at Phospholipid-decorated Surfaces of Liquid Crystals. *Science*, **2003**, *302*, 2094-2097.
- (10) Deng, J.; Liang, W.; Fang, J. Liquid Crystal Droplet-Embedded Biopolymer Hydrogel Sheets for Biosensor Applications. *ACS Appl. Mater. Interfaces* **2016**, *8*, 3928–3932.
- (11) Aliño, V. J.; Sim, P. H.; Choy, W. T.; Fraser, A.; Yang, K.-Y. Detecting Proteins in Microfluidic Channels Decorated with Liquid Crystal Sensing Dots. *Langmuir* **2012**, *28*, 17571–17577.
- (12) Lockwood, N. A.; Gupta, J. K.; Abbott, N. L. Self-assembly of Amphiphiles, Polymers and Proteins at Interfaces Between Thermotropic Liquid Crystals and Aqueous Phases. *Surf. Sci. Rep.* **2008**, *63*, 255-293.
- (13) Carlton, R. J.; Hunter, J. T.; Miller, D. S.; Abbasi, R.; Mushenheim, P. C.; Tan, L. N.; Abbott, N. L. Chemical and Biological Sensing using Liquid Crystals. *Liq. Cryst. Rev.* **2013**, *1*, 29-51.
- (14) Su, X.; Voskian, S. Russell, Hughes, P.; Aprahamian, I. Manipulating Liquid-Crystal Properties Using a pH Activated Hydrazone Switch. *Angew. Chem. Int. Ed.* **2013**, *52*, 10734-10739.
- (15) Miller, D. S.; Carlton, R. J.; Mushenheim, P. C.; Abbott, N. L. Introduction to Optical Methods for Characterizing Liquid Crystals at Interfaces. *Langmuir* **2013**, *29*, 3154-3169.
- (16) Eimura, H.; Miller, D. S.; Wang, X.; Abbott, N. L.; Kato, T. Self-Assembly of Bioconjugated Amphiphilic Mesogens Having Specific Binding Moieties at Aqueous-Liquid Crystal Interfaces. *Chem. Mater.* **2016**, *28*, 1170-1178.
- (17) Yang, K. L.; Cadwell, K.; Abbott, N. L. Contact Printing of Metal Ions onto Carboxylate- Terminated Self- Assembled Monolayers. *Adv. Mater.* **2003**, *15*, 1819-1823.
- (18) Shah, R. R.; Abbott, N. L. Orientational Transitions of Liquid Crystals Driven by Binding of Organoamines to Carboxylic Acids Presented at Surfaces with Nanometer-scale Topography. *Langmuir* **2003**, *19*, 275-284.

- (19) Abu-Abed, A.; Lindquist, R. G.; Choi, W.-H. Capacitive Transduction for Liquid Crystal-Based Sensors, Part I: Ordered System. *IEEE Sens. J.* **2007**, *7*, 1617-1624
- (20) Ho, W. F.; Chan, H. P.; Yang, K. L. Planar Optical Waveguide Platform for Gas Sensing Using Liquid Crystal. *IEEE Sens. J.* **2013**, *13*, 2521-2522.
- (21) Yang, K.-L.; Cadwell, K.; Abbott, N. L. Mechanistic Study of the Anchoring Behavior of Liquid Crystals Supported on Metal Salts and Their Orientational Responses to Dimethyl-methylphosphonate. *J. Phys. Chem. B* **2004**, *108*, 20180-20186.
- (22) Yang, K.-L.; Cadwell, K.; Abbott, N. L. Use of Self-assembled Monolayers, Metal ions and Smectic Liquid Crystals to Detect Organ-ophosphonates. *Sens. Actuators, B* **2005**, *104*, 50-56.
- (23) Cadwell, K. D.; Alf, M. E.; Abbott, N. L. Infrared Spectroscopy of Competitive Interactions Between Liquid Crystals, Metal Salts, and Dimethyl-methylphosphonate at Surfaces. *J. Phys. Chem. B* **2006**, *110*, 26081-26088.
- (24) Cadwell, K. D.; Lockwood, N. A.; Nellis, B. A.; Alf, M. E.; Willis, C. R.; Abbott, N. L. Detection of Organophosphorous Nerve Agents using Liquid Crystals Supported on Chemically Functionalized Surfaces. *Sens. Actuators, B* **2007**, *128*, 91-98.
- (25) Bungabong, M. L.; Ong, P. B.; Yang, K.-L. Using Copper Perchlorate Doped Liquid Crystals for the Detection of Organophosphonate Vapor. *Sens. Actuators, B* **2010**, *148*, 420-426.
- (26) Pal, S. K.; Acevedo-Vélez, C.; Hunter, J. T.; Abbott, N. L. Effects of Divalent Ligand Interactions on Surface-induced Ordering of Liquid Crystals. *Chem. Mater.* **2010**, *22*, 5474-5482.
- (27) Hunter, J. T.; Pal, S. K.; Abbott, N. L. Adsorbate-induced Ordering Transitions of Nematic Liquid Crystals on Surfaces Decorated with Aluminum Perchlorate Salts. *ACS Appl. Mater. Interfaces* **2010**, *2*, 1857-1865.
- (28) VanTreeck, H. J.; Most, D. R.; Grinwald, B. A.; Kupcho, K. A.; Sen, A.; Bonds, M. D.; Acharya, B. R. Quantitative Detection of a Simulant of Organophosphonate Chemical Warfare Agents Using Liquid Crystals. *Sens. Actuators, B* **2011**, *158*, 104-110.
- (29) Wang, P.-H.; Yu, J.-H.; Zhao, Y.-B.; Li, Z.-J.; Li, G.-Q. A Novel Liquid Crystal-based Sensor for the Real-time Identification of Organophosphonate Vapors. *Sens. Actuators, B* **2011**, *160*, 929-935.
- (30) Hunter, J. T.; Abbott, N. L. Dynamics of the Chemo-optical Response of Supported Films of Nematic Liquid Crystals. *Sens. Actuators, B* **2013**, *183*, 71-80.
- (31) Lai, Y.-T.; Kuo, J.-C.; Yang, Y.-J. Polymer-dispersed Liquid Crystal Doped with Carbon Nanotubes for Dimethyl-methylphosphonate Vapor-sensing Application. *Appl. Phys. Lett.* **2013**, *102*, 191912.
- (32) Hunter, J. T.; Abbott, N. L. Adsorbate-Induced Anchoring Transitions of Liquid Crystals on Surfaces Presenting Metal Salts with Mixed Anions. *ACS Appl. Mater. Interfaces* **2014**, *6*, 2362-2369.
- (33) Li, G.; Gao, B.; Yang, M.; Chen, L.-C.; Xiong, X.-L. Homeotropic Orientation Behavior of Nematic Liquid Crystals Induced by Copper Ions. *Colloids Surf.*, B 2015, 130, 287-291.
- (34) Robinson, S. E.; Grinwald, B. A.; Bremer, L. L.; Kupcho, K. A.; Acharya, B. R.; Owens, P. D. A Liquid Crystal-Based Passive Badge for Personal Monitoring of Exposure to Hydrogen Sulfide. *J. Occup. Environ. Hyg.* **2014**, *11*, 741-750.

- (35) Roling L. T.; Scaranto, J.; Herron, J. A.; Yu, H.; Choi, S.; Abbott, N. L.; Mavrikakis, M. Towards First-principles Molecular Design of Liquid Crystal-based Chemoresponsive Systems. *Nat. Commun.* **2016**, *7*, 13338.
- (36) Gaussian 09, Revision D.01, Frisch, M. J.; Trucks, G. W.; Schlegel, H. B.; Scuseria, G. E.; Robb, M. A.; Cheeseman, J. R.; Scalmani, G.; Barone, V.; Mennucci, B.; Petersson, G. A.; Nakatsuji, H.; Caricato, M.; Li, X.; Hratchian, H. P.; Izmaylov, A. F.; Bloino, J.; Zheng, G.; Sonnenberg, J. L.; Hada, M.; Ehara, M.; Toyota, K.; Fukuda, R.; Hasegawa, J.; Ishida, M.; Nakajima, T.; Honda, Y.; Kitao, O.; Nakai, H.; Vreven, T.; Montgomery, J. A., Jr.; Peralta, J. E.; Ogliaro, F.; Bearpark, M.; Heyd, J. J.; Brothers, E.; Kudin, K. N.; Staroverov, V. N.; Kobayashi, R.; Normand, J.; Raghavachari, K.; Rendell, A.; Burant, J. C.; Iyengar, S. S.; Tomasi, J.; Cossi, M.; Rega, N.; Millam, J. M.; Klene, M.; Knox, J. E.; Cross, J. B.; Bakken, V.; Adamo, C.; Jaramillo, J.; Gomperts, R.; Stratmann, R. E.; Yazyev, O.; Austin, A. J.; Cammi, R.; Pomelli, C.; Ochterski, J. W.; Martin, R. L.; Morokuma, K.; Zakrzewski, V. G.; Voth, G. A.; Salvador, P.; Dannenberg, J. J.; Dapprich, S.; Daniels, A. D.; Farkas, Ö.; Foresman, J. B.; Ortiz, J. V.; Cioslowski, J.; Fox, D. J. Gaussian, Inc., Wallingford CT, 2009.
- (37) Perdew, J. P.; Chevary, J. A.; Vosko, S. H.; Jackson, K. A.; Pederson, M. R.; Singh, D. J.; Fiolhais, C. Atoms, Molecules, Solids, and Surfaces: Applications of the Generalized Gradient Approximation for Exchange and Correlation. *Phys. Rev. B* **1992**, *46*, 6671-6687.
- (38) Weigend, F.; Ahlrichs, R. Balanced Basis Sets of Split Valence, Triple Zeta Valence and Quadruple Zeta Valence Quality for H to Rn: Design and Assessment of Accuracy. *Phys. Chem. Chem. Phys.* **2005**, 7, 3297-3305.
- (39) Zhao, Y.; Truhlar, D. G. The M06 Suite of Density Functionals for Main Group Thermochemistry, Thermochemical Kinetics, Noncovalent Interactions, Excited States, and Transition Elements: Two New Functionals and Systematic Testing of Four M06-class Functionals and 12 Other Functionals. *Theor. Chem. Account* **2008**, *120*, 215-241.
- (40) Inorganic Chemistry (5th Edition), Eds.: Gary L. Miessler, Paul J. Fischer and Donald A. Tarr, Prentice Hall, 2013.
- (41) McDonnell, D. G.; Raynes, E. P.; Smith, R. A. Dipole-moments and Dielectric-properties of Fluorine Substituted Nematic Liquid Crystals. *Lig. Cryst.* **1989**, *6*, 515-523.
- (42) Inukai, T.; Kondo, Y.; Sato, H.; Saito, H.; Sugimori, S. 4'-Al-kyl-4-fluorobiphenyls; Jpn. Patent; JP 56.150.030 (1981/11/20); 1981.
- (43) Bedolla Pantoja, M. A.; Abbott. N. L. Surface-controlled Orientational Transitions in Elastically Strained Films of Liquid Crystal That Are Triggered by Vapors of Toluene." *ACS Appl. Mater. Interfaces* **2016**, *8*, 13114-13122.
- (44) Miller, D. S.; Carlton, R. J.; Mushenheim, P. C.; Abbott, N. L. Introduction to Optical Methods for Characterizing Liquid Crystals at Interfaces. *Langmuir* **2013**, *29*, 3154-3169.
- (45) Hunter, J. T.; Abbott, N. L. Dynamics of the Chemo-optical Response of Supported Films of Nematic Liquid Crystals. *Sens. Actuators*, B **2013**, *183*, 71-80.
- (46) Szabo, A.; Ostlund, N. S. Modern Quantum Chemistry: Introduction to Advanced Electronic Structure Theory. Dover Books, 1996.



Supporting Information

Design of Chemoresponsive Liquid Crystals through Integration of Computational Chemistry and Experimental Studies

Tibor Szilvási[†], Luke T. Roling[†], Huaizhe Yu[†], Prabin Rai[‡], Sangwook Choi[†], Robert J. Twieg^{‡,*}, Manos Mavrikakis^{†,*}, Nicholas L. Abbott^{†,*}

[†] Department of Chemical and Biological Engineering, University of Wisconsin-Madison, 1415 Engineering Drive, Madison, Wisconsin 53706-1607, USA.

[‡] Department of Chemistry and Biochemistry, Kent State University, Kent, Ohio 44242, USA.

Fabrication of polymeric microwells. Polymeric wells with diameters of 200 µm were fabricated by photolithography to create LC films supported on metal salt surfaces (as detailed below). A schematic illustration of the steps to fabricate the microwells is presented in Fig. S1. SU-8 2005, which contains 45 wt% bisphenol A novolac epoxy, was made by adding cyclopentanone to SU-8 2050, which contains 71.65 wt% bisphenol A novolac epoxy, to decrease the viscosity of the photoresist. Then, a thin film of SU-8 2005 was deposited on a cleaned glass surface by spincoating at 500 rpm for 10 s followed by 3,000 rpm for 30 s. The polymer-coated surface was subsequently prebaked on a hot plate at 95 °C for 5 min and then cooled to room temperature for 10 min. After prebaking, a photomask with 200 μm-diameter dark circular patterns was placed on the polymer coated surface and exposed to UV for 70 s ($\lambda = 254$ nm, UV crosslinker, Spectronics, Westbury, NY). After UV exposure, the sample was post-baked for 7 min at 95 °C. The polymer film was placed into a desiccator to which 25 µl of (tridecafluoro-1,1,2,2-tetrahydrooctyl)trichlorosilane was added (adjacent to the polymer film). A vacuum was then pulled in the dessicator for 20 min, during which time the organosilane formed a vapor and reacted with the surface of the polymer film. After the surface treatment, the sample was placed in a SU-8 developer (1-methoxy-2-propyl acetate) and sonicated for 15 s to dissolve the regions of the SU-8 film that were not exposed to UV light. The sample was then washed with a copious amount of isopropanol and dried with under a gaseous flow of nitrogen. The depth of the polymeric microwells fabricated using the abovementioned procedure was determined to be 5µm by surface profilometry.1

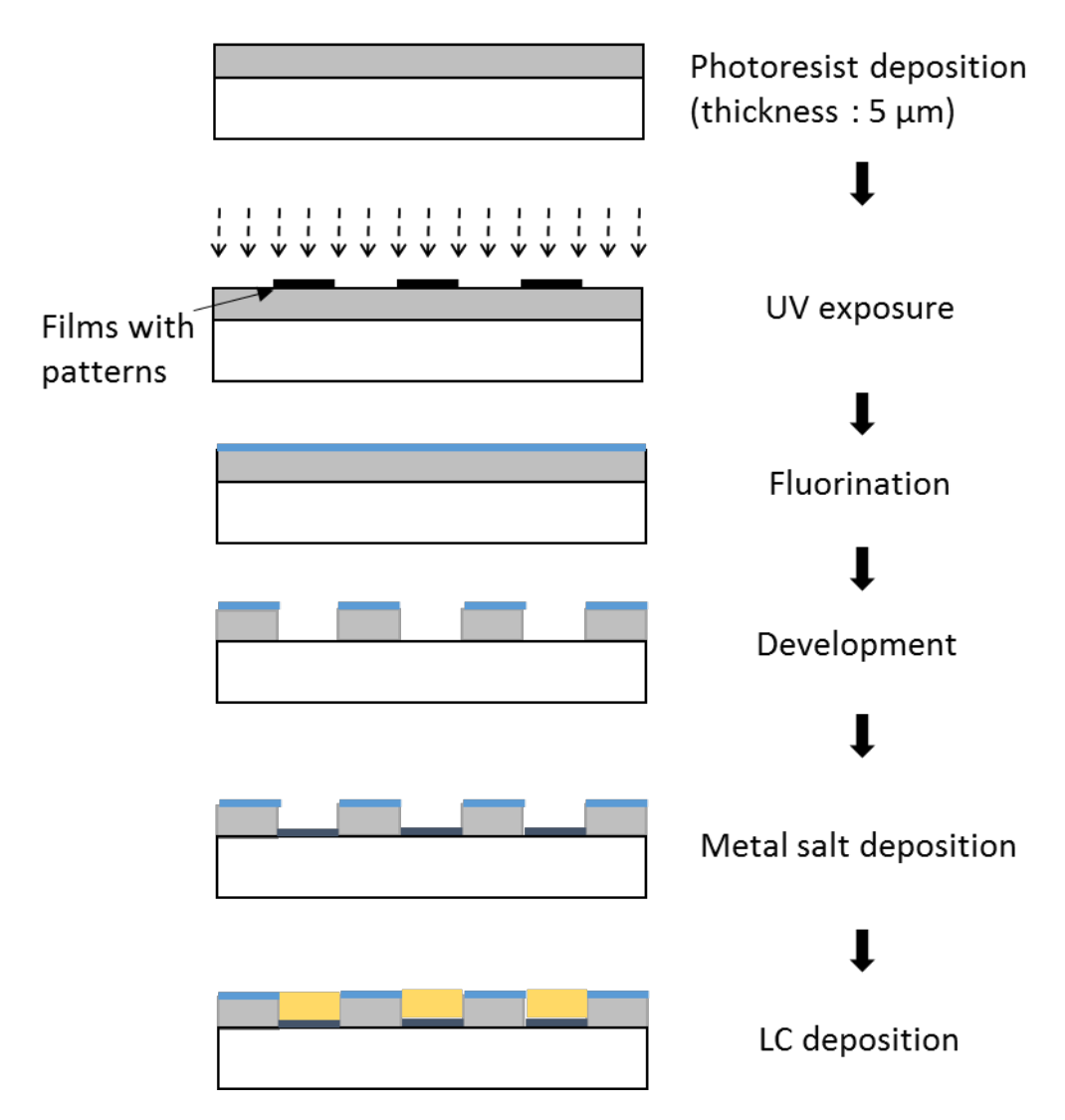


Figure S1. Process for the fabrication of microwells and preparation of LC thin films supported on metal salts within microwells

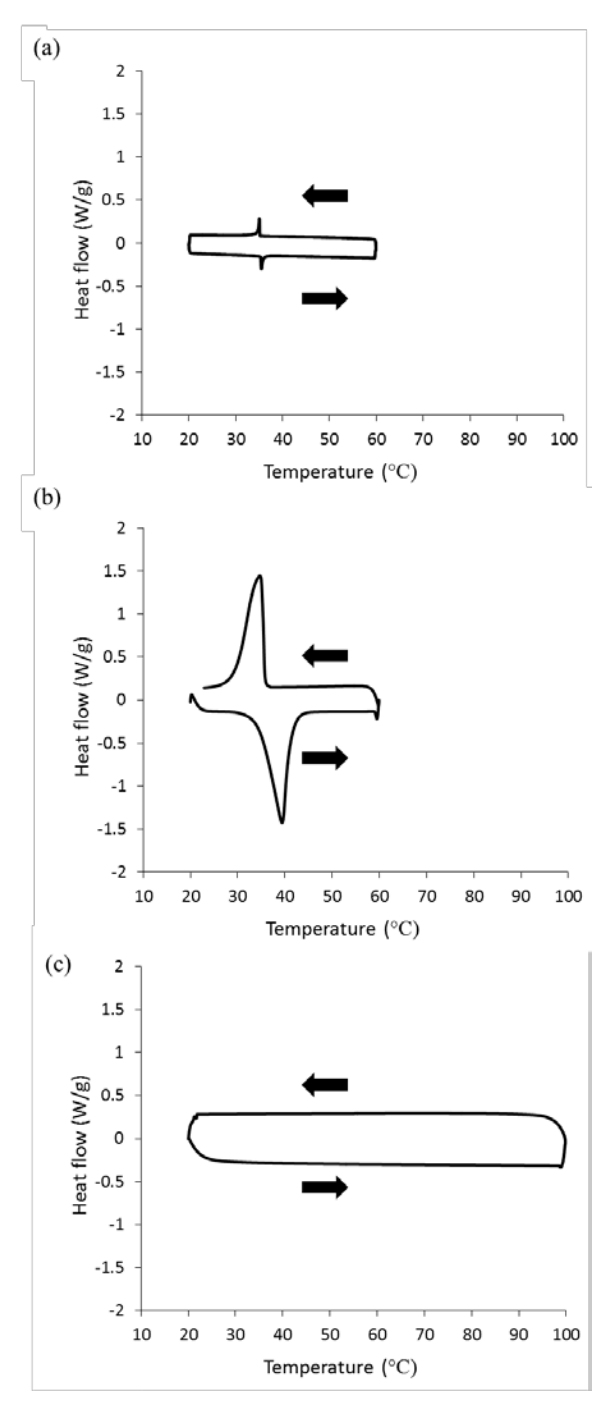


Figure S2. Differential scanning calorimetry of (a) 5CB, (b) F1, and (c) FCB. The 5CB exhibits a phase transition from nematic to isotropic phase at 35.5 °C. F1 changes from solid to liquid phase at 39 °C, but it does not have a LC phase. FCB is a liquid state at room temperature and there is no phase change between 20 °C and 100 °C, and it does not have a LC phase. As the arrows indicate the bottom line corresponds to heating while the upper line corresponds to cooling. DSC scan rate 2 °C/min.

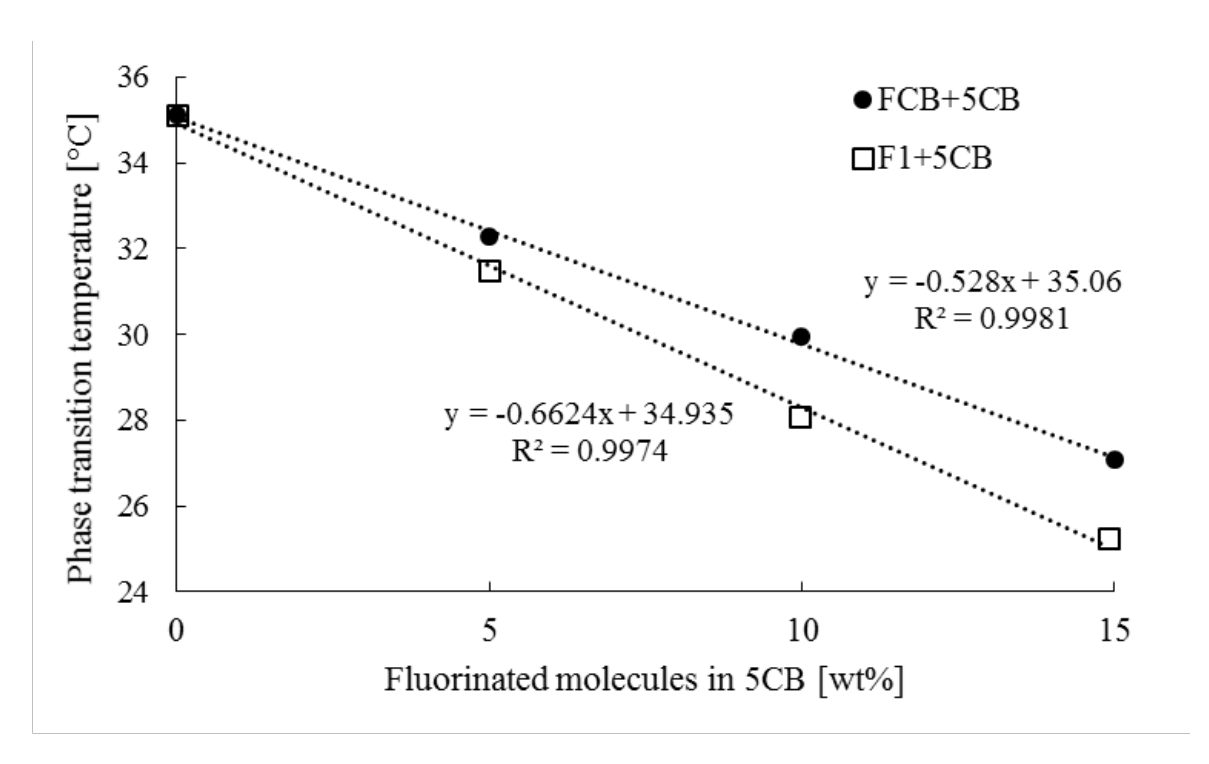


Figure S3. Phase transition temperature between nematic and isotropic phase of F1 or FCB mixed with 5CB. Error bars are smaller than the symbols indicating the measured results.

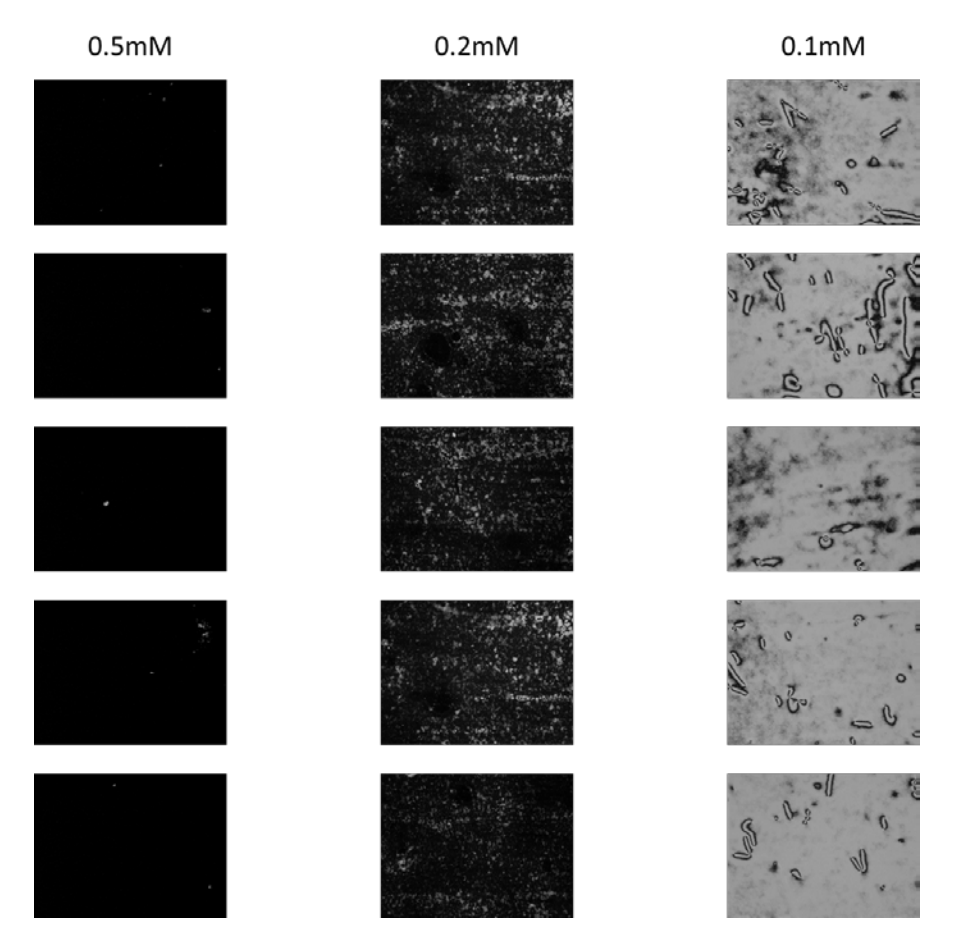


Figure S4. Five optical images of pure 5CB held between two symmetric iron salt deposited substrates using 0.5 mM, 0.2 mM or 0.1 mM Fe(ClO₄)₃ solutions.

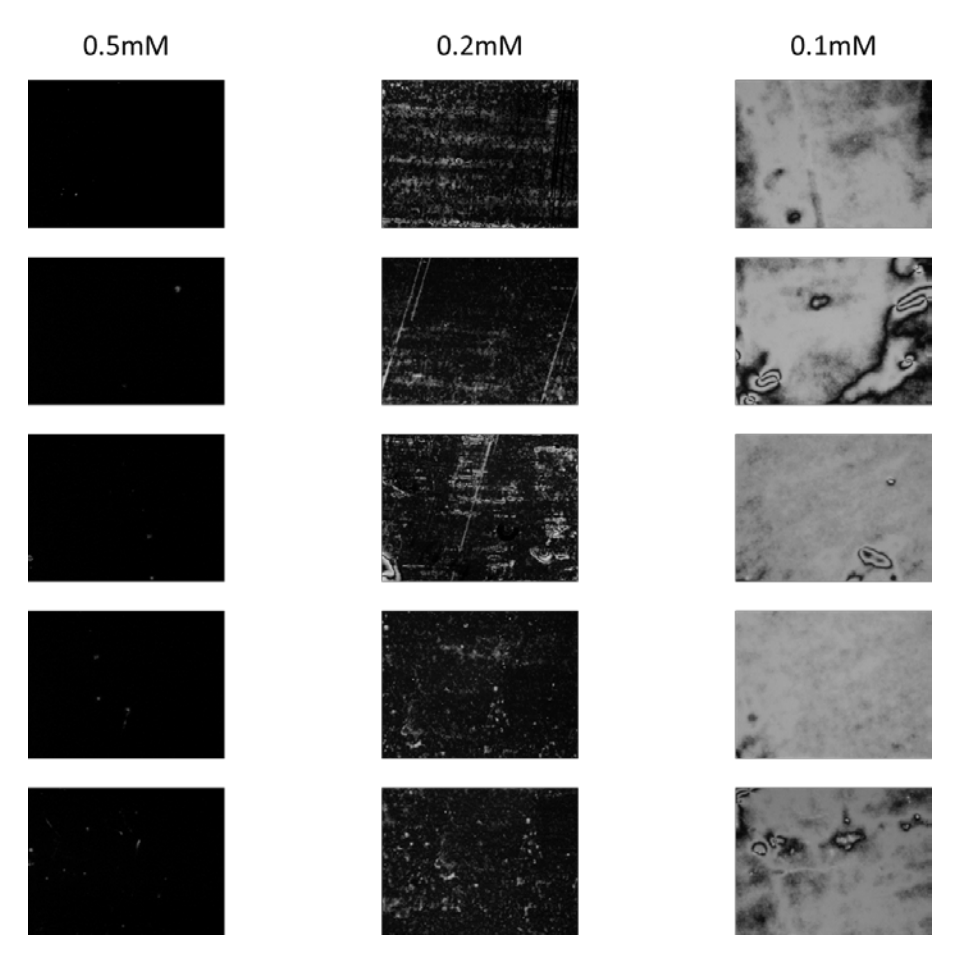


Figure S5. Five optical images of F1 mixture (95 wt% 5CB + 5 wt% F1) held between two symmetric iron salt deposited substrates using 0.5 mM, 0.2 mM or 0.1 mM Fe(ClO₄)₃ solutions.

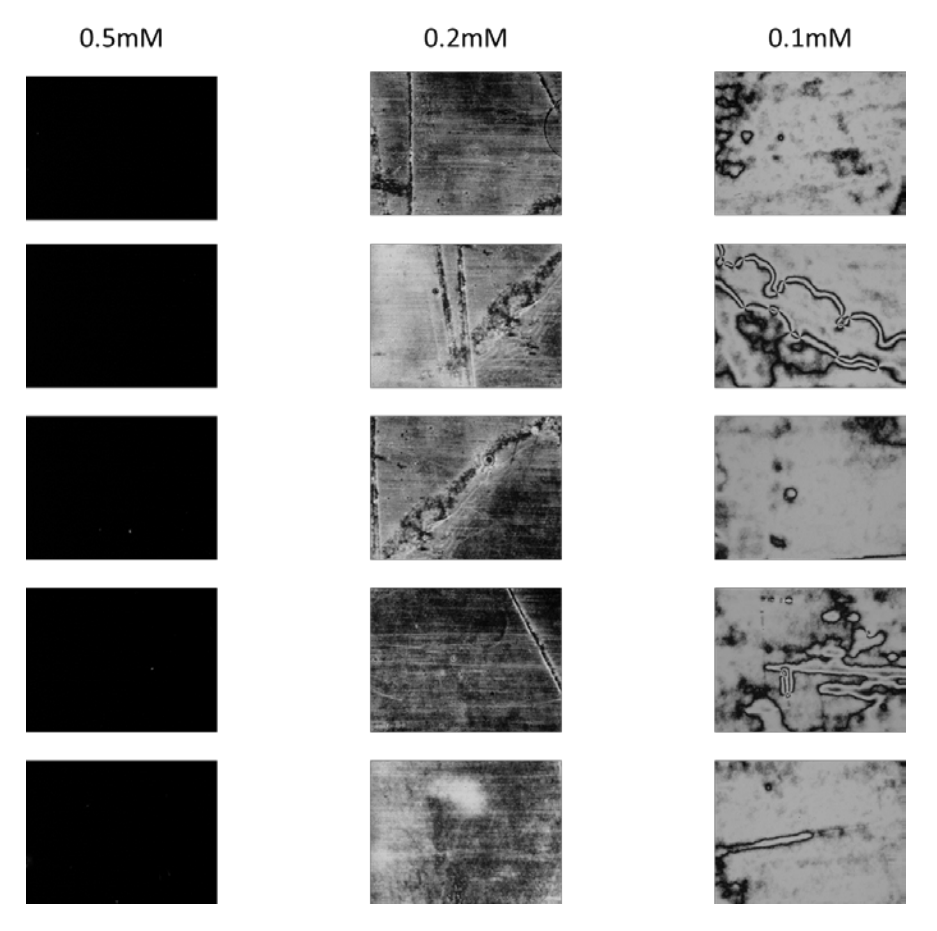
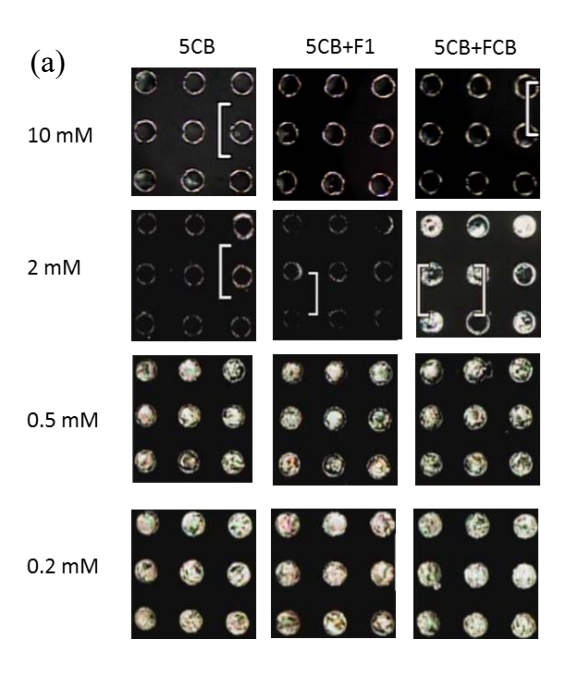


Figure S6. Five optical images of FCB mixture (95 wt% 5CB + 5 wt% FCB) held between two symmetric iron salt deposited substrates using 0.5 mM, 0.2 mM or 0.1 mM Fe(ClO₄)₃ solutions.



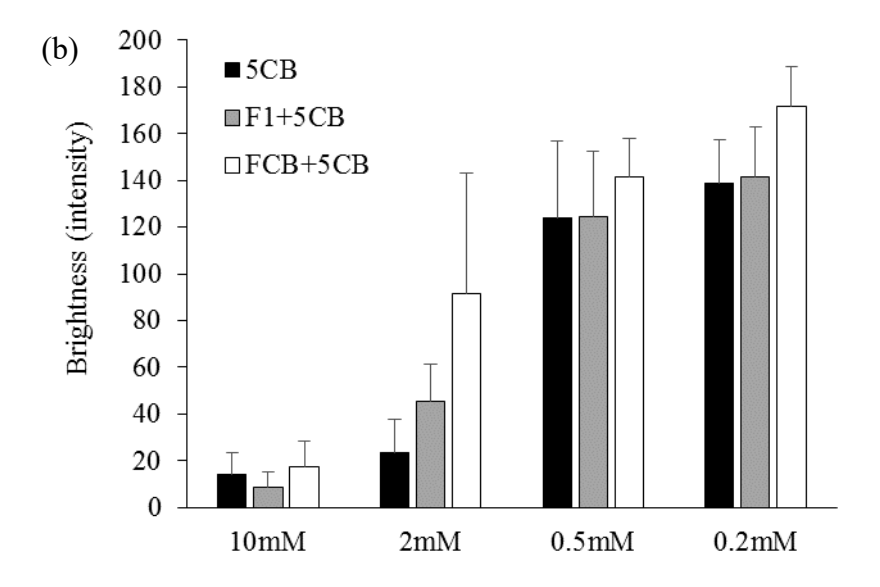


Figure S7. (a) Optical images of pure 5CB, F1 mixture (95 wt% 5CB + 5 wt% F1) and FCB mixture (95 wt% 5CB + 5 wt% FCB) supported on Fe(ClO₄)₃ salts within microwells. The salts were deposited on the bottom of microwells using 0.2 - 10 mM Fe(ClO₄)₃ solutions. (b) Intensity of optical images of 5CB, 5CB doped with 5 wt% F1 (5CB+F1), and 5CB doped with 5 wt% FCB (5CB+FCB) supported on Fe(ClO₄)₃ salts hosted within arrays of wells according to the concentration of bulk solutions.

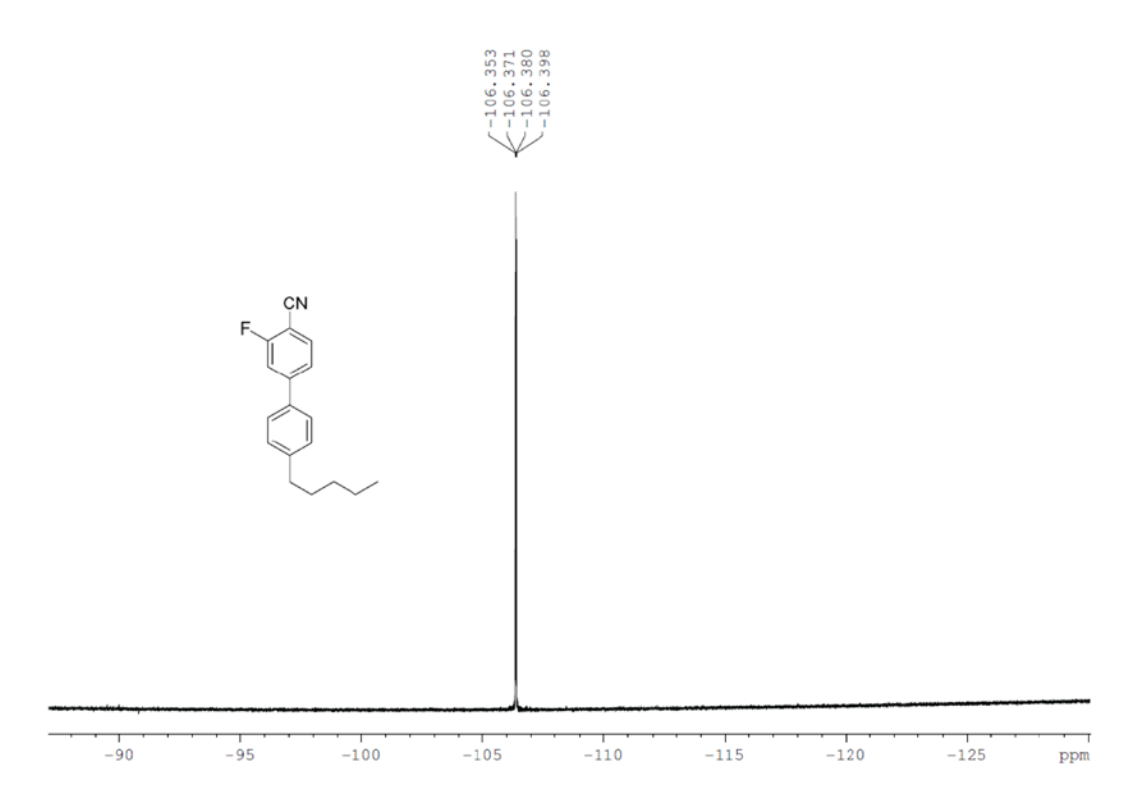


Figure S8. ¹⁹F NMR spectrum of FCB.

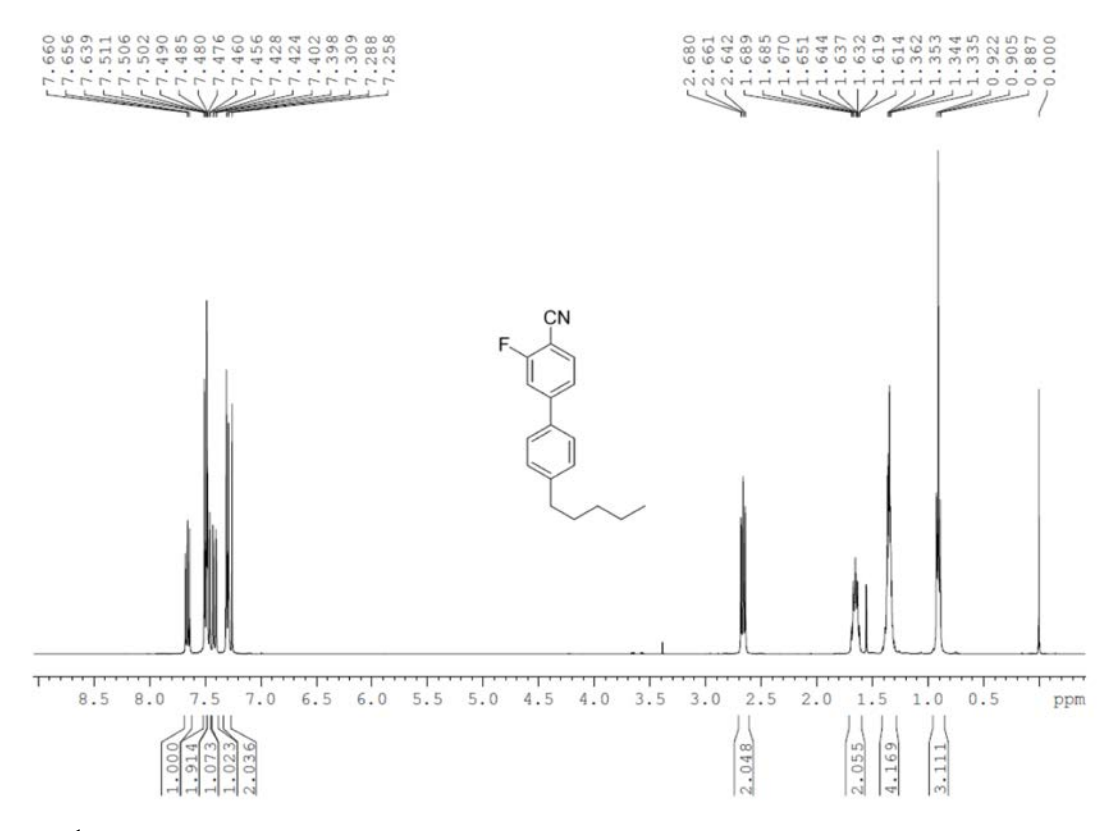


Figure S9. ¹H NMR spectrum of FCB.

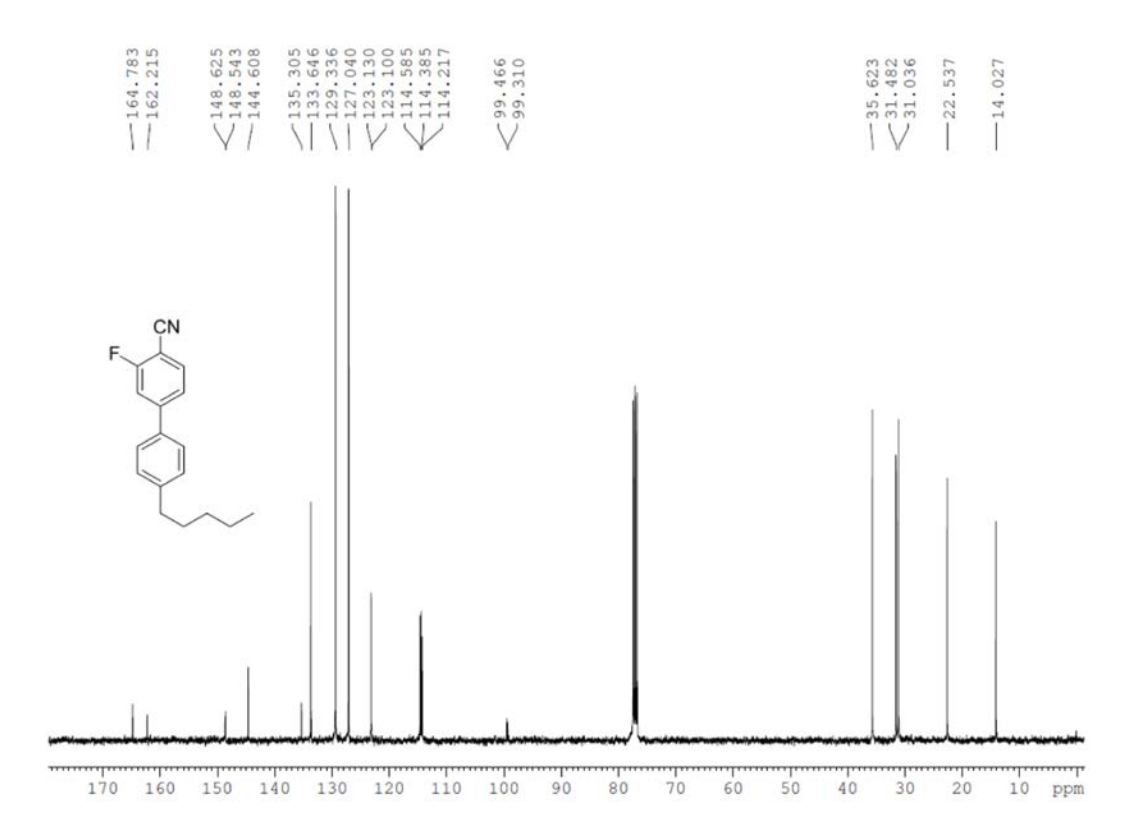


Figure S10. ¹³C NMR spectrum of FCB.

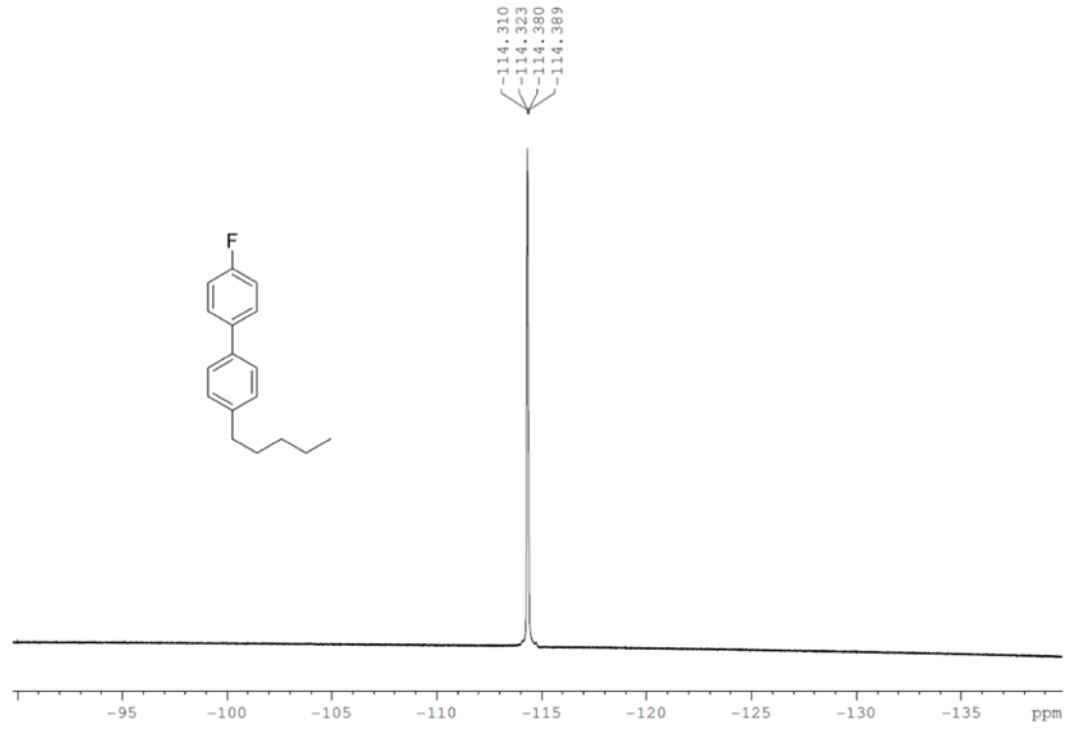


Figure S11. ¹⁹F NMR spectrum of F1.

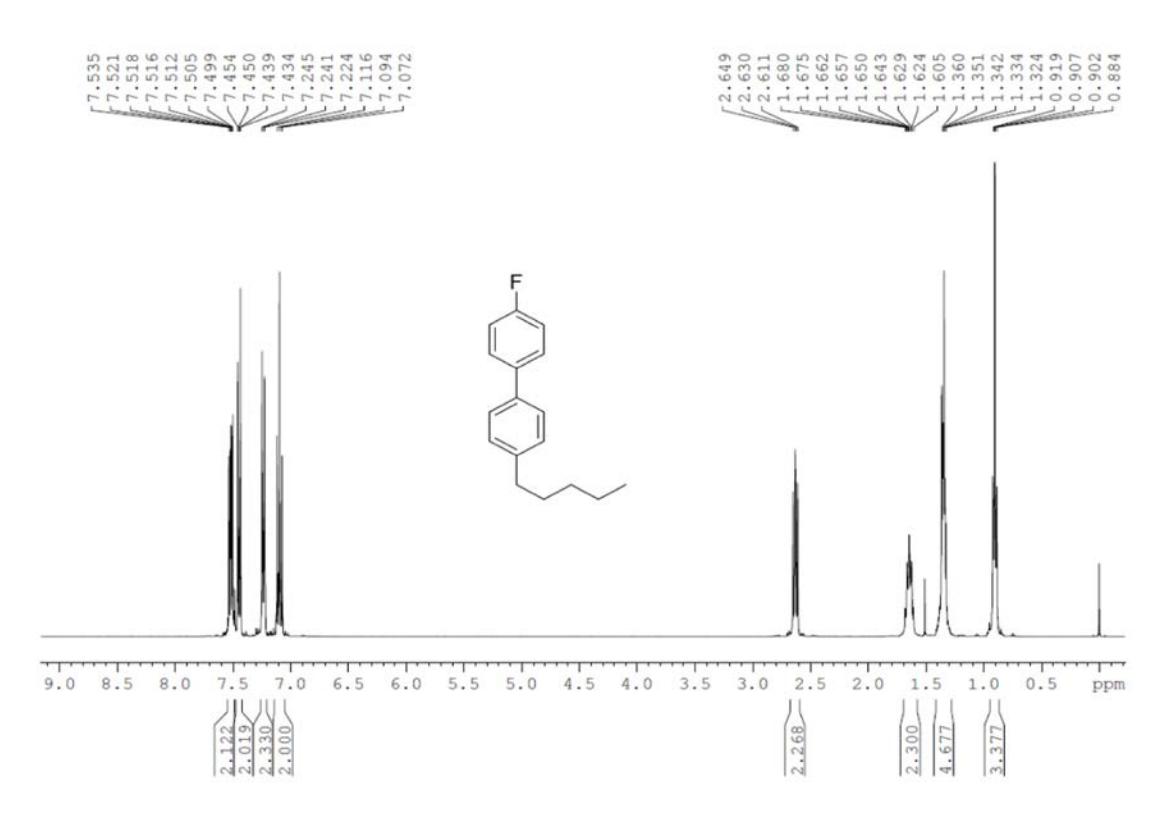


Figure S12. ¹H NMR spectrum of F1.

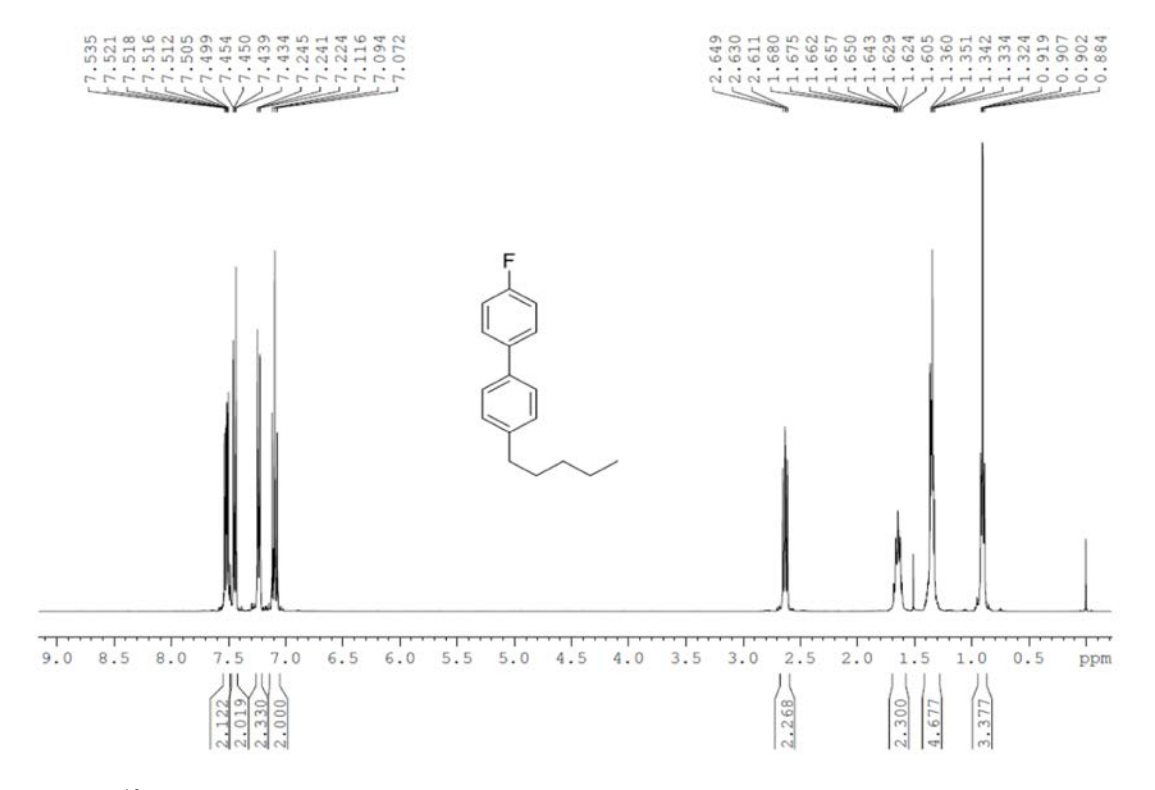


Figure S13. ¹³C NMR spectrum of F1.

References

1. Bedolla Pantoja, M.A.; Abbott, N.L., Surface-Controlled Orientational Transitions in Elastically Strained Films of Liquid Crystal that are Triggered by Vapors of Toluene, *Applied Materials & Interfaces*, **2016**, 8(20), 13114-13122.